

Article

Acidic and Electrosurface Properties of Binary TiO₂-SiO₂ Xerogels Using EPR of pH-Sensitive Nitroxides

Denis O. Antonov ^{1,*} , Daria P. Tamasova ¹, Andrey B. Shishmakov ², Igor A. Kirilyuk ³ 
and Elena G. Kovaleva ¹

¹ Institute of Chemical Engineering, Ural Federal University Named after the First President of Russia B N Yeltsin, Mira St., 19, 620002 Yekaterinburg, Russia; d.p.tamasova@urfu.ru (D.P.T.); e.g.kovaleva@urfu.ru (E.G.K.)

² Laboratory of Organic Materials, I. Ya. Postovsky Institute of Organic Synthesis, Ural Branch of the Russian Academy of Sciences, Akademicheskaya/S. Kovalevskoy, 22/20, 620990 Ekaterinburg, Russia; Mikushina@ios.uran.ru

³ Institute of Organic Chemistry, Siberian Branch of the Russian Academy of Sciences, Akad. Lavrent'ev Av. 9, 630090 Novosibirsk, Russia; kirilyuk@nioc.nsc.ru

* Correspondence: d.o.antonov@urfu.ru

Abstract: The binary xerogels TiO₂-SiO₂ are widely used as catalysts and their carriers in organic synthesis. Characterization and adjustment of the electrostatic properties of the surface and the local acidity inside the pores, are necessary for the further development of TiO₂-SiO₂ xerogels applications. This research investigates acid–base equilibria in the pores, and the surface electrostatic potential (SEP) of binary TiO₂-SiO₂ xerogels, by the EPR of stable pH-sensitive nitroxide radicals. These radicals are small enough to penetrate directly into the pores, and to be adsorbed onto the surface of the material under study. This makes it possible to obtain valuable information on the acidic and electrosurface properties of the studied system. The highest negative surface electrical charge associated with surface electrical potential (SEP) was equal to -196 ± 6 mV. It was induced by the surface of the sample with a 7% TiO₂ content. The local acidity inside the pores of this sample was found to be higher, by approximately 1.49 pH units, as compared to that in the external bulk solution.

Keywords: xerogels characterization; TiO₂-SiO₂; surface electrostatic potential; electron paramagnetic resonance; pH-sensitive nitroxide radicals; titration curve



Citation: Antonov, D.O.; Tamasova, D.P.; Shishmakov, A.B.; Kirilyuk, I.A.; Kovaleva, E.G. Acidic and Electrosurface Properties of Binary TiO₂-SiO₂ Xerogels Using EPR of pH-Sensitive Nitroxides. *Gels* **2021**, *7*, 119. <https://doi.org/10.3390/gels7030119>

Academic Editor: Ashleigh Fletcher

Received: 25 June 2021

Accepted: 6 August 2021

Published: 11 August 2021

Publisher's Note: MDPI stays neutral with regard to jurisdictional claims in published maps and institutional affiliations.



Copyright: © 2021 by the authors. Licensee MDPI, Basel, Switzerland. This article is an open access article distributed under the terms and conditions of the Creative Commons Attribution (CC BY) license (<https://creativecommons.org/licenses/by/4.0/>).

1. Introduction

The binary SiO₂-TiO₂ xerogels have been applied in a variety of fields of science and technology. These materials are widely used in optical waveguides and sensors [1], hydrophilic coatings, selective sorbents for purification of air [2,3], and aqueous media [4] made from organic and inorganic compounds [5–7], and in self-purifying materials, based on glass [8] or cotton [9]. They have been successfully applied as carriers of catalysts in the Fischer–Tropsch process [10] and various oxidation reactions [11], as well as a matrix for the immobilization of the biomacromolecules and components of drug delivery systems [12]. Cu(II)-containing TiO₂-SiO₂ xerogels were investigated and found to be efficient photocatalysts [13]. Polyfunctional heterogeneous systems, based on Cu(II)-containing titanium dioxide, were proven to consist of various self-organized copper-containing structures, which are catalytically active in the reactions of hydroxyarene oxidation [14–17].

At present, the sol-gel technology is widely used as a method of synthesis, based on the reactions that were developed by Nikolaon and Teichner in 1976, to obtain silica aerogels [18]. These are the reactions of the hydrolysis and gelation of alkoxides or other reactive compounds in an alcohol solution, with the addition of acids and alkalis as catalysts.

It was found that in different processes utilizing these xerogels, the acidity of the solutions contacting with them plays an important role; however, the pH values of the

external solution (pH_{ext}) can differ from that of the solution inside pores (pH_{loc}). The reasons for these differences can be the changes both in the intrinsic electrical charge of the surface and in the properties of the surface water.

The acidity and electro-surface properties of the surface are determined by the number and type of functional groups of the materials, and depend on the synthesis conditions and phase composition [19]. The surface of silica were found to have five types of functional groups, in different proportions [20].

Previous relevant studies have shown that the classical methods of surface acidity measurement are mostly based on the spectrophotometric studies of adsorbed dyes (Hammett indicators) during titration, or the measurements of microcalorimetry and the temperature-programmed desorption of other basic and/or acidic probes of various strengths, to estimate the concentration and strength of acidic sites [19,21,22]. Several spectroscopic techniques, including conventional infrared (IR) and Fourier transform infrared (FTIR) spectroscopy, magic angle rotation NMR and electron paramagnetic resonance (EPR), ultraviolet (UV), visible and photoluminescence spectroscopy, Raman scattering, and X-ray radiation photoelectron spectroscopy, have been used effectively for the identification of some catalytic mesoporous materials and the characterization of the acid–base properties of different surface locations [11,23].

These spectroscopic methods have their advantages and disadvantages. EPR spectroscopy of ionizable nitroxides is especially useful in the investigation of opaque or turbid materials [24–26]. The EPR of spin probes exhibits better concentration sensitivity compared to solid-state NMR. The EPR method is based on the spectroscopic observation of the reversible protonation of stable free radicals, e.g., pH-sensitive nitroxide radicals (NR) [27] or triarylmethyl radicals [28].

Electron paramagnetic resonance (EPR) is a physical phenomenon that is observed in molecular systems possessing unpaired electronic spins. This phenomenon involves the absorption of electromagnetic radiation of a frequency that is found to be in resonance with the gyroscopic precession of the spins' magnetic moments, occurring in a static magnetic field. The resonance condition can be reached by scanning either the magnetic field or frequency; technical reasons make it easier to sweep the magnetic field. The most common way to detect EPR is the continuous wave (CW) EPR experiment, in which the magnetic field is changed, while the frequency is kept constant. EPR spectroscopy is a versatile and exceptionally sensitive technique for detecting and studying molecular systems possessing unpaired electronic spins [25]. The scope of EPR applications in analytical chemistry can be significantly expanded by using spin labels and spin probes, that is, paramagnetic species introduced to gain information on the system. To be suitable for analytical applications, spin labels and probes should immediately report on the properties of interest, produce ERP signals that are distinguishable from the background, and leave the system only minimally perturbed by their presence [25]. The EPR spectroscopy of pH-sensitive spin probes is based on the observation of nitroxide radicals that contain basic nitrogen functionalities in the heterocyclic ring. The protonation of these functionalities changes the intermolecular electric field, which, in turn, affects the nitroxide magnetic parameters, such as nitrogen hyperfine coupling A-tensor and g-factor matrix, as reflected by the nitroxide CW EPR spectra [27]. These phenomena make the EPR spectra of such nitroxides exceptionally sensitive to local pH (pH_{loc}) values [28]. As the method is based on EPR detection, it is fully applicable to opaque and not transparent samples, such as the nano and mesoporous materials that are studied in this research.

The general objective of this work was to investigate the surface electrostatic potential (SEP), surface charge, and pH_{loc} of the binary intrinsic and annealed TiO_2 - SiO_2 systems with different titanium contents, using continuous wave (CW) X-band (9 GHz) EPR and a pH-sensitive nitroxide radical (4-dimethylamino-2-ethyl-5,5-dimethyl-2-(pyridine-4-yl)-2,5-dihydro-1H-imidazol-1-oxyl) as a spin probe.

2. Results and Discussion

2.1. Xerogels Characterization

The morphology of the oxide xerogels was examined by SEM. Figure 1 shows the SEM micrographs of the samples $\text{TiO}_2(7\%)\text{-SiO}_2$. The images demonstrate porous structure synthesis samples.

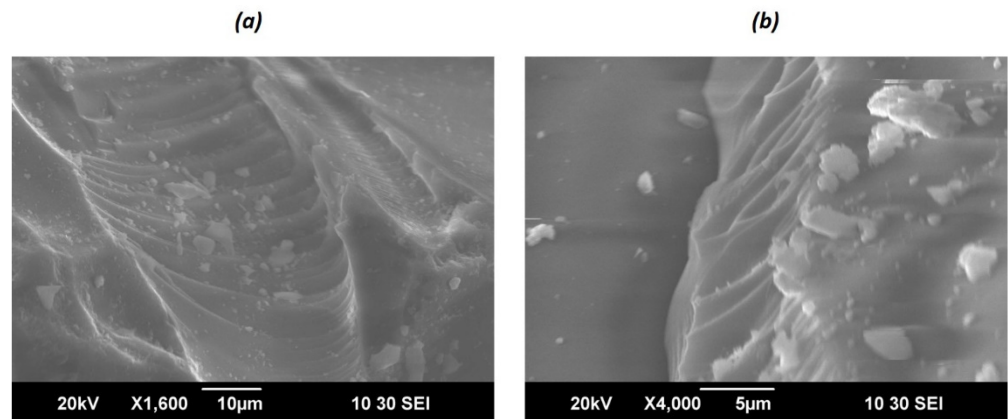


Figure 1. SEM image of $\text{TiO}_2(7\%)\text{-SiO}_2$ samples. Metric scale (a) 10 μm and (b) 5 μm in 1 cm of the image.

The infrared spectrum of the SiO_2 xerogel (Figure 2a) had an intense complex-shaped absorption band, with the maxima at 1155 and 1062 cm^{-1} , and an absorption band with a maximum at 798 cm^{-1} corresponding to stretching vibrations of Si–O–Si bonds.

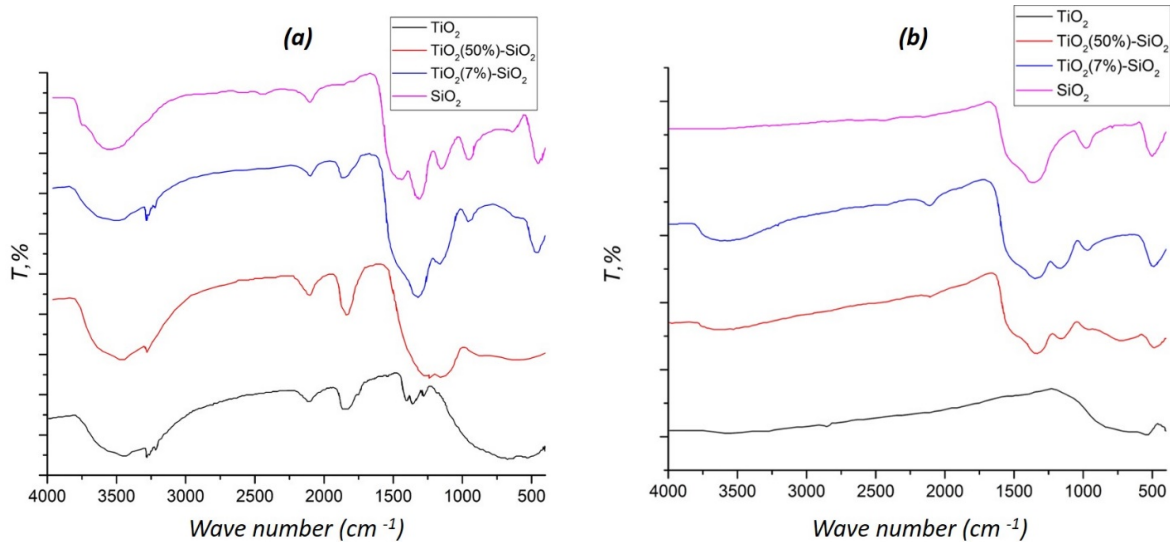


Figure 2. FT-IR spectra of synthesized xerogels (a) before and (b) after annealing at 850 $^{\circ}\text{C}$.

The complex-shaped band corresponded to asymmetric stretching vibrations and the average intensity band at 798 cm^{-1} to symmetric stretching vibrations of SiO_4 tetrahedra. The absorption band with a maximum at 945 cm^{-1} demonstrated symmetric stretching vibrations of nonbridging Si–O– bonds. An intense band at 435 cm^{-1} corresponded to the bending vibrations of polyhedra. The absorption bands of stretching vibrations of surface hydroxyl groups and water appeared to be in the range of 3700–3000 cm^{-1} . A broadband of average intensity in the region of 1626 cm^{-1} corresponded to the bending vibrations of water [29]. The ratios of the intensities of the absorption bands of Ti–O–Si and Si–O–Si groups at 950 cm^{-1} and 1079 cm^{-1} , respectively, for binary oxide xerogels as a function

of the oxide xerogels composition are shown in Table 1. These data demonstrated that the number of Ti–O–Si groups decreased with increasing titanium oxide fraction of the binary system.

Table 1. Characteristics of the synthesized binary TiO₂-SiO₂ xerogels.

TiO ₂ Content, %	S, m ² /g	Ratio of the Absorption Band IR Intensities of Ti–O–Si and Si–O–Si Groups at 950 cm ⁻¹ and 1079 cm ⁻¹
0	27.8	0
7	254.3	0.5
50	16.4	0.2
100	0.7	0

Annealing at 850 °C (Figure 2b) caused dehydroxylation of the SiO₂ sample, as evidenced by the absence of absorption bands at 3700–3000 cm⁻¹, and the non-bridging Si–O–bonds in the spectra. Similarly, in titanium dioxide, due to calcination, the absorption bands of the Ti–OH groups (1126, 1095, and 1036 cm⁻¹) were also not found. In the spectra of binary xerogels and TiO₂, water absorption bands (3700–3000 cm⁻¹, 1625 cm⁻¹) were present, which was the result of sorption from the atmosphere, due to the hygroscopicity of the samples.

2.2. Rotational Motion of Spin Probes in Individual Oxides and Binary Oxide Xerogels

The acid-base characteristics of water in the micropores of inorganic oxides and ion-exchange resins, are known to differ from those in the external solution [30]. To measure the pH_{loc} inside the pores of the samples, the pH-sensitive spin-probe technique was used [24]. We evaluated the SEP of individual and binary oxide xerogels, and its effect on the acidity of the solution inside the pores in the samples.

At a pH_{ext} below 10, the experimental EPR spectra of NR in the TiO₂-SiO₂ and SiO₂ samples represented a superposition of isotropic and anisotropic signals (Figure 3), indicating the coexistence of two forms of NR, with different molecular mobilities. The isotropic signal (Figure 3, highlighted in magenta) corresponds to the fast-motioned NR molecules that are located in a diffusion layer inside the pores [31]. The signals produced by the NR molecules allow information on the acidity of the solution inside the pores of oxide materials to be obtained [30,32]. The anisotropic signal (Figure 3, highlighted in blue and green) was generated by the NR molecules that were adsorbed onto the surface. This signal provides information on SEP [33].

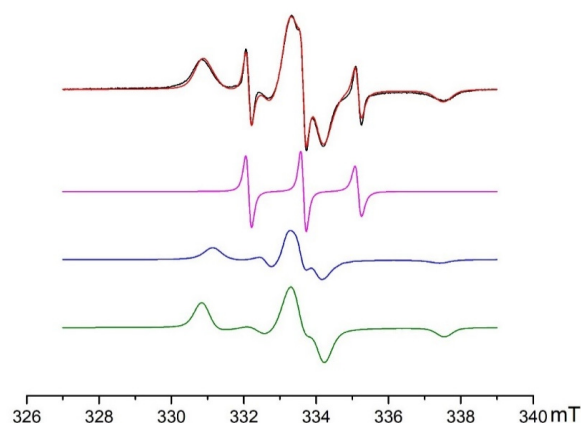


Figure 3. Experimental (black curve) and simulated (red curve) EPR spectra of the NR on the surface of the TiO₂(7%)-SiO₂ binary system at $pH_{ext} = 5.58$. The simulated EPR spectrum of the NR is a superposition of three signals, namely, fast-motioned NR (magenta curve), slow-motioned NR in the protonated (blue curve), and non-protonated forms (green curve).

At a pH_{ext} value greater than 10, only the isotropic EPR signal characteristic of fast-motivated NR, which was located inside the pores of the oxide xerogels, was recorded.

The NR that was adsorbed on the TiO_2 surface only gave isotropic spectra for all the pH_{ext} values.

2.3. EPR Titration of NR in the Individual and Binary Intrinsic Oxides

EPR titration curves of the NR in external aqueous solution, as well as in SiO_2 and binary TiO_2 - SiO_2 xerogels, are shown in Figure 4. For NR in external aqueous solution, the isotropic hyperfine splitting constant (HFS) was plotted vs. the pH_{ext} . The fraction of the slow-motion component of NR inside the pores was determined via EPR spectra simulation, and was used as a pH-dependent parameter for the investigation of SiO_2 and binary TiO_2 - SiO_2 xerogels.

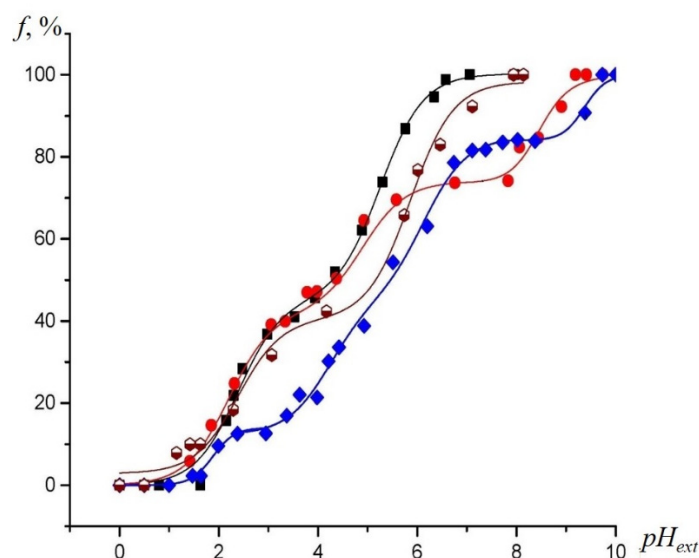


Figure 4. Experimental EPR titration curves for the NR at 293 K obtained by plotting the fast- and slow-motivated component of the EPR spectra of the NR in the non-protonated form (f) vs. pH_{ext} in aqueous solution (**black squares**), and inside the SiO_2 (**red circles**), TiO_2 (50%)- SiO_2 , (**brown hexagons**) and TiO_2 (7%)- SiO_2 , (**blue diamonds**), respectively.

The upper part of the titration curve for the SiO_2 sample was found to be shifted to the right (to the higher pH_{ext} values), relatively to the EPR titration curves of the NR in external aqueous solution (the black curve), which indicated a negative charge of the silicon dioxide surface in a neutral and weakly acidic solution (at $pH_{ext} > 3-4$) [30,33]. As the value of pH_{ext} decreased, the EPR titration curve for this oxide came closer to the calibration curve and intersected it, thus shifting to the left, relatively to that at a pH_{ext} less than three. It is known that the hydroxylated silica surface has point of zero charges (PZC) at pH_{ext} values between two and three, and becomes charged positively at the lesser value pH_{ext} [34].

The horizontal plateaus in the titration curves of the NR inside SiO_2 , and the TiO_2 - SiO_2 binary xerogels obtained by simulating the anisotropic spectra, reflected the invariance of the fraction of the non-protonated form of the NR, f , with a change in pH_{ext} . These plateaus were explained by the ionization of the silicon dioxide silanol groups [33]. The pK_a values of functional groups can be measured by projecting any pH-sensitive parameter of an EPR spectrum of the NR inside the material corresponding to a horizontal plateau on the calibration curve, and then to the pH_{ext} axis [33]. In our case, the pH-sensitive parameter was f (Figure 4).

For the binary TiO_2 (7%)- SiO_2 samples, the EPR titration curves of the NR showed a greater shift to the right (to the higher pH_{ext} values) from the calibration curve, as compared to the curve for the individual SiO_2 , indicating the stronger negative charge of the pores

surface at high values of pH_{ext} . The existence of a plateau in the pH_{ext} range of 2.5–3.5 indicated the formation of new acidic centers with a higher acidity than that of the silanol groups in the individual SiO_2 . As a result of the deprotonation of these groups at higher pH_{ext} values, the surface acquired a negative charge (SEP). This charge caused a decrease in the acidity of the remaining silanol groups, shifting the plateau in the upper part of the titration curve further upwards (to the higher pH_{ext} region). Remarkably, the titration of the TiO_2 (50%)- SiO_2 sample showed a much lower shift of the titration curve to the right (the surface became charged negatively). We noted that a buildup of the titanium dioxide content in the samples led to an increase in the dissociation constant of the silanol groups, since the upper plateau on the titration curve for NR in the TiO_2 (7%)- SiO_2 sample was positioned above that for pristine SiO_2 . We assumed that for the TiO_2 (50%)- SiO_2 sample, the titration of silanol groups would take place at the pH_{ext} values above the sensitivity range of the NR used. Therefore, we did not observe the characteristic plateau on the titration curve for this sample. Interestingly, the EPR titration curve of the NR was shifted higher to the right for a binary system with a 7% mol of TiO_2 content. The IR spectroscopy data (Table 1), which indicated the maximum amount of the mixed phase for this sample, allowed us to conclude that an increase in the negative surface charge for this sample is associated precisely with the formation of a mixed Ti–O–Si phase.

The plateau in the titration curves of the NR in binary oxides in the pH_{ext} value range from 2.5 to 4.5, corresponds to the deprotonation of either the silanol groups of the silica located near titanium atoms or new functional groups arising in the mixed Ti–O–Si phase. It proved the presence of the mixed Ti–O–Si phase, along with the individual phases of SiO_2 and TiO_2 in the binary TiO_2 - SiO_2 xerogels, by the NMR method, and it was noted that the functional groups that were associated with the mixed-phase showed higher acidity than the silanol ones [35]. These groups, with similar values of pK_a , were revealed in the study of binary ZrO_2 - SiO_2 oxide xerogels, which indicated that they (groups) belonged to a mixed phase [36].

2.4. EPR Titration of NR in the Individual and Binary Annealed Oxides

The annealing of SiO_2 samples at 850 °C led to the formation of multiple acidic centers on the sample surface, and resulted in the shift of the titration curve to the right at a pH_{ext} value range of 4–5.5. At the higher pH_{ext} values, these centers were ionized, providing the negative SEP, which in turn decreased the acidity of the remaining silanol groups. As a result, further ionization of these silanol groups occurs at the higher pH_{ext} values, with the titration curve plateau shifting upwards. We observed that the shift of the titration curve for the NR in the annealed sample at $pH_{ext} > 8$, was found to be lesser than that for the sample before annealing. This effect was due to the partial decomposition of acidic silanol groups, which led to a decrease in the total negative charge of the surface (SEP) at alkaline pH_{ext} .

Specifically, the increase in the pK_a value of silanol functional groups, after annealing at 850 °C, was attributed to the fact that upon completion of the titration in the annealed sample, SEP became greater (in absolute value) than that for the unannealed one (Figure 5, green curve). Within the pH_{ext} range from four to seven, the curve is positioned at the right, relatively to the red curve. Hence, the dissociation of silanol groups (removal of the positively charged hydrogen H^+ ions) in these samples was impeded not only by the bond strength in the acid group Si–O–H, but also by the increased negative charge of the entire matrix of the sample. An increase in the negative charge of the silicon oxide surface after calcination can be associated with the formation of both siloxane groups on the silicon oxide surface and Lewis acid sites. This is due to the detachment of silanol groups during heat treatment.

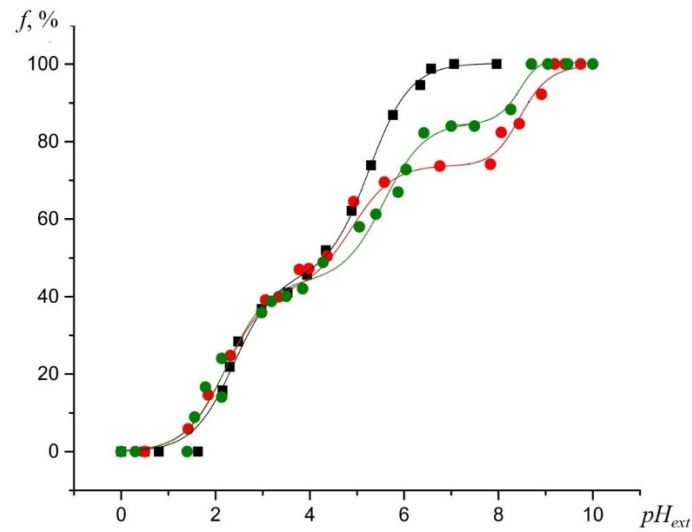


Figure 5. Experimental EPR titration curves for the NR at 293 K obtained by plotting the fast- and slow-motioned component of the EPR spectra of the NR in the non-protonated form (f) vs. pH_{ext} in aqueous solution (**black squares**) and inside the SiO_2 (red circles), SiO_2 annealed at 850 °C (**green circles**), respectively.

In contrast, annealing of the binary TiO_2 - SiO_2 samples at 850 °C did not lead to a decrease in the total number of ionized groups at alkaline pH_{ext} values (Figure 6). Thus, the TiO_2 additive increased the thermal stability of the silanol groups. However, strongly acidic groups present only in binary oxides, and providing a plateau in the titration curve at pH 2–4 completely disappeared from the sample surface. Acidic centers that are similar to those observed in the annealed SiO_2 were formed, instead of exhibiting on the titration curve plateau at the pH_{ext} value of 2.5–4.5. The dissociation constants of the functional groups before and after calcination were found to be equal to 1.90 ± 0.08 and 2.90 ± 0.08 , respectively.

A broad singlet in the EPR spectra of the NR appeared only for the annealed TiO_2 (50%)- SiO_2 sample. This occurred due to the presence of coal that formed as a result of burning the organic fraction of the precursors retained in the sample pores [29].

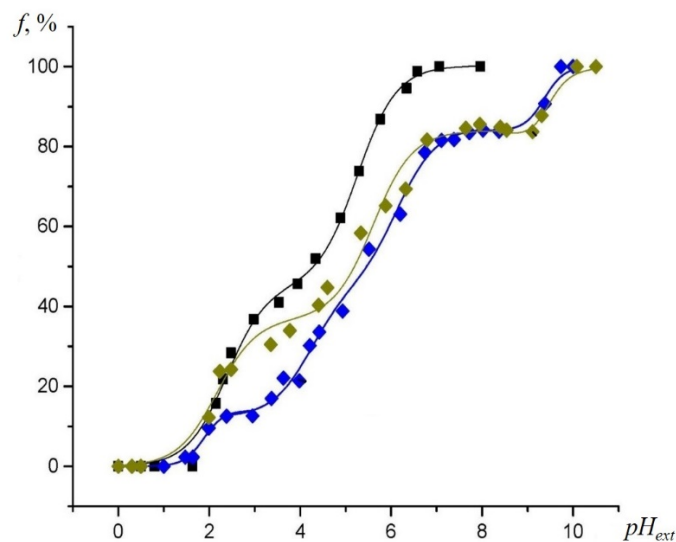


Figure 6. Experimental EPR titration curves for the NR at 293 K were obtained by plotting the fast- and slow-motioned component of the EPR spectra of the NR in the non-protonated form (f) vs. pH_{ext} in aqueous solution (**black squares**), and inside the TiO_2 (7%)- SiO_2 (**blue diamonds**), TiO_2 (7%)- SiO_2 annealed at 850 °C (**green diamonds**), respectively.

2.5. Effect of Incorporation of Cu(II) Ions into the Binary Oxides on EPR Titration of NR for Cu(II)-Containing Binary Xerogels

The incorporation of Cu(II) into TiO₂-SiO₂ samples allowed partial compensation for the negative charge, with a pronounced shift of the titration curve to the left, as shown in Figure 7. The dissociation constants of the functional groups (*pK_a* values) of different oxide xerogels, and the highest SEP of their surface (in absolute value), are shown in Table 2. The decrease in the *pK_a* can be associated with the decline in the negative charge of the sample matrix. It facilitated the dissociation of the silanol groups, and, as a result, the plateau in the titration curve was shifted down to the lower *pH_{ext}* values.

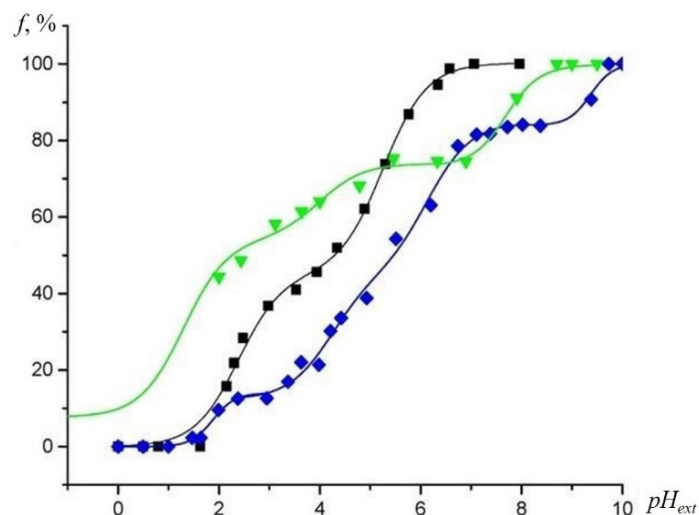


Figure 7. Experimental EPR titration curves for the NR at 293 K obtained by plotting the fast- and slow-motivated component of the EPR spectra of the NR in the non-protonated form (*f*) vs. *pH_{ext}* in aqueous solution (**black squares**) and inside the TiO₂ (7%)-SiO₂ (**blue diamonds**), TiO₂-SiO₂-Cu(II) (**green triangles**), respectively.

Table 2. Acid–base and electrostatic characteristics of the samples studied.

Sample	<i>pK_a</i> of Functional Groups ± 0.08		ΔpK^{el} ± 0.08	SEP ± 6 mV
SiO ₂	5.30	-	2.73	-159
TiO ₂ (7%)-SiO ₂ -	5.60	1.90	3.37	-196
TiO ₂ (50%)-SiO ₂ -	-	3.20	0.73	-42
SiO ₂ annealed	5.70	-	2.36	-137
TiO ₂ (7%)-SiO ₂ - annealed	5.60	2.90	3.50	-204
TiO ₂ (7%)-SiO ₂ -Cu(II)	5.30	-	1.97	-115

As was mentioned above, no signal in the EPR spectrum for immobilized NR was observed in the TiO₂ samples. However, titration of the fast-motivated NR molecules near the TiO₂ and SiO₂ surfaces led to similar *a*, % vs. *pH_{ext}* dependences (Figure 8) (*a* is the pH-sensitive parameter, characterizing the hyperfine coupling constant, HFS constant).

The EPR titration curves for the dissolved NR near the surface of the SiO₂ samples were significantly shifted to the right, relatively to the titration curve for the NR in the bulk aqueous solution. The shift is more noticeable at a *pH_{ext}* less than 4.5, which can be ascribed to an increased acidity of the solution inside the samples' pores, compared to the *pH_{ext}* [30], due to the surface charge (close to zero) of *pH_{ext}* (Figure 4). The highest shift of the EPR titration curves for the NR to the right, relatively to that in the bulk aqueous solution, was observed in the TiO₂ (7%)-SiO₂ sample (Figures 4 and 8). The surface charge affects the acid–base equilibrium of the NR in a solution inside the pores.

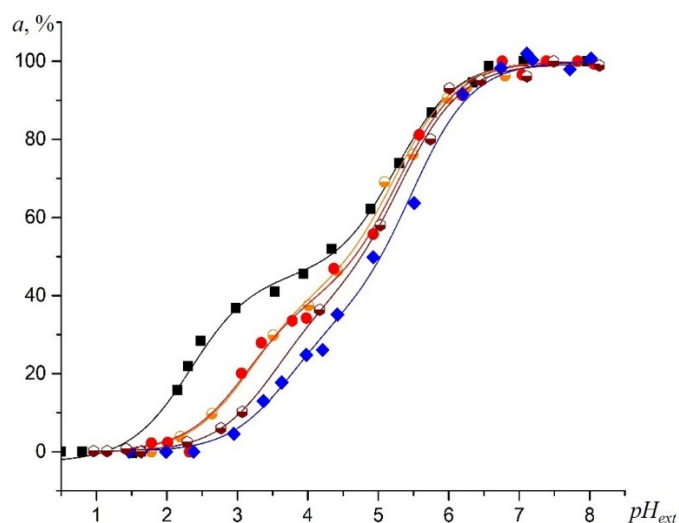


Figure 8. Experimental room-temperature EPR titration curves for the NR obtained by plotting isotropic nitrogen HFS, a vs. pH_{ext} at ionic strength $I = 0.1$ M (**black squares**) and reporting on the average acidity inside the pores of TiO_2 (**orange circles**), SiO_2 (**red circles**), TiO_2 (7%)- SiO_2 (**blue diamonds**), TiO_2 (50%)- SiO_2 (**wine hexagons**).

The differences between pH_{ext} and pH_{loc} in the oxide xerogels are shown in Table 3.

Table 3. The differences in pH_{ext} and pH_{loc} for the oxide xerogels.

Sample	$\Delta pH = pH_{ext} - pH_{loc}$	
	$pH_{ext} \leq 4.5$	$pH_{ext} \geq 4.5$
SiO_2	−0.82	−0.1
TiO_2 (7%)- SiO_2	−1.49	−0.37
TiO_2 (50%)- SiO_2	−1.21	−0.17
TiO_2	−0.84	−0.04

3. Conclusions

CW X-band EPR spectroscopy of a pH-sensitive nitroxide radical, used as a free-motivated or adsorbed spin probe, was applied to study acid–base equilibria in the pores and surfaces of TiO_2 - SiO_2 binary xerogels that were prepared by a sol-gel technique in the wet ammonia vapors atmosphere. The results showed that the variation in the composition of binary xerogels led to a change in both the electrosurface and acidic properties of the materials studied.

The new acidic centers, with a higher acidity than silanol groups, were formed in the binary system TiO_2 (7%)- SiO_2 . Moreover, these samples showed a higher content of acidic groups on the surface, hence, the higher negative surface electrical potential compared to the pure silica samples (−196 to −204 mV vs. −137 to −159 mV). The local acidity inside the sample's pores was found to increase by approximately 1.49 pH units, as compared to the bulk external solution. The annealing of pure silicon oxide at 850 °C decreased the number of silanol groups on the surface and increased the value of the dissociation constant of these groups. While the calcination of the TiO_2 (7%)- SiO_2 sample did not affect a decrease in the number of silanol groups, the breakdown of strongly acidic groups in the substituted oxide was observed.

4. Materials and Methods

4.1. Materials

Tetraethoxysilane 98% (TEOS), tetrabutoxytitanium 99% (TBT) precursors were purchased from Alfa Aesar (USA) and used without further purification.

The stable nitroxide radical 4-dimethylamino-2-ethyl-5,5-dimethyl-2-(pyridine-4-yl)-2,5-dihydro-1H-imidazol-1-oxyl used as a pH-sensitive spin probe, was synthesized according to previously described protocol [27].

4.2. Synthesis of Binary TiO_2 - SiO_2 Xerogels

The synthesis of the samples was carried out by the sol-gel technique, according to the protocol previously described in [29], using titanium and silicon alkoxides as precursors. The hydrolysis of the samples was performed in presence of wet ammonia vapors.

Samples with 7% and 50% TiO_2 were obtained by mixing TBT and TEOS in ratios of 1:9 and 6:4, respectively. The synthesis was carried out in porcelain dishes with a round bottom, 60 mm in diameter and 30 mL in volume. To synthesize the SiO_2 and TiO_2 individual oxides, 10 mL of TBT or TEOS were subjected to hydrolysis. The dish was placed into a 3 L desiccator containing a beaker with 100 mL of 10% aqueous ammonia and stored until hydrolysis was complete. After hydrolysis, the samples were dried for 48 h at room temperature, then kept in a drying oven at 90 °C for 24 h. Some samples were calcined annealed in a quartz reactor at a temperature of 850 °C (heating rate 10 °C/min) in air flow with a rate of 0.075 m³/h for an hour.

The TiO_2 (7%)- SiO_2 -Cu (II) samples were obtained by dissolving 0.01 g of $\text{CuCl}_2 \times 2\text{H}_2\text{O}$ in the appropriate TEOS/TBT mixture with a subsequent treatment, according to the protocol above.

Compact FT-IR spectrometer: ALPHA II (manufacturer: Bruker Optics) was used for FT-IR measurements in the wavenumber range from 4000 to 400 cm⁻¹. Scanning electron microscope (SEM) images were obtained by using a Carl Zeiss EVO LS 10 device (manufacturer: Carl Zeiss NTS, Jena, Germany).

4.3. EPR-Based Spin Probe Method for Measuring Acid–Base and Electrosurface Properties

Potentiometric titration of powdered individual and binary oxides in the range of pH_{ext} from 1 to 10 was carried out by a conventional batch multi-sample technique [30,37]. Titration was carried out at 293 K with 0.1 N solutions of acid (HCl) and alkali (NaOH).

The samples were kept in the NR solution with a concentration of 1×10^{-4} M for 2 h to establish dynamic equilibrium between the external bulk solution and the solution inside solid phase. Thereafter, pH values of the equilibrium pH_{ext} were measured by a 3-in-1 combination pH electrode and a Mettler Toledo FP20 pH meter (Mettler-Toledo, Columbus, OH, USA) with the specified accuracy of ± 0.01 pH. The ± 0.01 pH error was significantly less than typical errors of ± 0.05 pH units arising from the analysis of EPR titration curves and, therefore, were neglected. After the residual powder was filtered off and compressed between filter papers to remove excess liquid, the sample was placed inside the quartz EPR tube (i.d. = 3.5 mm), and EPR spectra were recorded immediately thereafter. Sealing of the samples inside the quartz tube prevented water evaporation from the pores. Detailed descriptions of EPR titration experiments and analysis of EPR spectra can be found in [26,31,38].

All EPR spectra were recorded at room temperature (≈ 293 K) using the X-band CW Bruker Elexys E-500 EPR spectrometer. Aqueous solutions of NR were positioned into open-end quartz capillaries with i.d. = 0.50 mm and o.d. = 0.70 mm (VitroCom Inc., Mountain Lakes, NJ, USA), the ends of the capillary were sealed with Critoseal® (Leica Microsystems Inc., Buffalo Grove, IL), and placed in a standard quartz tube (i.d. = 3.5 mm). The tube was consequently inserted into an EPR resonator.

All EPR titrations were carried out in a solution of $I = 0.1$ M. Errors of the individual measurements for NR in the bulk aqueous phase were ± 0.002 mT while for NR confined inside xerogels those values were ± 0.004 mT. To record the EPR spectra, the optimal conditions of microwave power and amplitude of modulation of the magnetic field were chosen.

4.4. Titration Curves Plotting

Further processing of the experimental spectra was carried out using J. Freed's software [39] and Microcal OriginPro 2015. The experimental hyperfine coupling constant (HFS) characterized by parameter $a, \%$ was plotted against pH_{ext} .

The dissociation constants of the functional groups of the NR used were calculated from the Henderson–Hasselbalch Equation (1) for dibasic acids, as follows:

$$a = (P_1 + P_2 \times 10^{pKa1 - pH} + P_3 \times 10^{pKa1 + pKa2 - 2pH}) / (1 + 10^{pKa1 - pH} + 10^{pKa1 + pKa2 - 2pH}) \quad (1)$$

where P_1 , P_2 , and P_3 are parameters that correspond to the HFS constants of the radical (a_N) in different ionization states of RH_2^{++} , RH^+ , and R , respectively; pKa_1 , pKa_2 , and pKa_3 are the antilogarithms of the ionization constants for RH_2^{++} , RH^+ , and R , respectively; a is the HFS constant.

The electro-surface properties were obtained from the analysis of the anisotropic signal of the NR EPR spectra. The change in the fraction of the non-protonated form (f) of the NR adsorbed on the surface of the solid-phase material was monitored in the range of pH_{ext} from 1 to 10, as follows:

$$f = n_R / (n_R + n_{RH_2^{++}}) \quad (2)$$

where n_R and $n_{RH_2^{++}}$ are the fractions of slow-motioned radical molecules in the non-protonated form and the protonated form, respectively.

4.5. SEP Calculation

In the case of the pH-sensitive probe adsorbed on the surface of the material under study, Khramtsov et al. in [24] established a relationship between the surface potential and the ionization constant of pH-sensitive NR, as follows:

$$\Delta pK_a^{el} = -(e \times \varphi / 2.3) \times k \times T \quad (3)$$

where ΔpK_a^{el} is the shift in pK_a of the NR in the sample induced by an electric potential; e is an electron charge; φ —electrostatic potential, mV; k is the Boltzmann constant; T is the temperature, K.

Author Contributions: D.O.A.: conceptualization, methodology, validation, formal analysis, investigation, writing—original draft, supervision, funding acquisition. E.G.K.: conceptualization, methodology, validation, formal analysis, writing of the original draft, supervision, project administration, funding acquisition. D.P.T.: investigation. A.B.S.: resources, methodology, investigation. I.A.K.: resources, methodology, investigation, formal analysis, writing of the original draft, funding acquisition. All authors have read and agreed to the published version of the manuscript.

Funding: D.O.A., E.G.K., D.P.T. acknowledge the financial support from the Russian Foundation for Basic Research (RFBR) grant 18-29-12129mk, I.A.K. acknowledges support from the Ministry of Science and Education of the Russian Federation grant No. 14.W03.31.0034 for the nitroxide synthesis.

Acknowledgments: The authors are thankful to late Leonid S. Molochnikov (1948–2020) for fruitful ideas, productive discussions of all the results obtained and for his help with the manuscript preparation.

Conflicts of Interest: The authors declare no conflict of interest.

References

1. Song, C.F.; Lü, M.K.; Yang, P.; Xu, D.; Yuan, D.R. Structure and photoluminescence properties of sol–gel TiO₂–SiO₂ films. *Thin Solid Films* **2002**, *413*, 155–159. [CrossRef]
2. Li, Y.; Wang, W.-N.; Zhan, Z.; Woo, M.-H.; Wu, C.-Y.; Biswas, P. Photocatalytic reduction of CO₂ with H₂O on mesoporous silica supported Cu/TiO₂ catalysts. *Appl. Catal. B Environ.* **2010**, *100*, 386–392. [CrossRef]
3. Obuchi, E.; Sakamoto, T.; Nakano, K.; Shiraiishi, F. Photocatalytic decomposition of acetaldehyde over TiO₂/SiO₂ catalyst. *Chem. Eng. Sci.* **1999**, *54*, 1525–1530. [CrossRef]
4. Rasalingam, S.; Peng, R.; Koodali, R.T. Removal of Hazardous Pollutants from Wastewaters: Applications of TiO₂–SiO₂ Mixed Oxide Materials. *J. Nanomater.* **2014**, *2014*, 1–42. [CrossRef]

5. Li, Y.; Murphy, P.; Wu, C.-Y. Removal of elemental mercury from simulated coal-combustion flue gas using a SiO₂-TiO₂ nanocomposite. *Fuel Process. Technol.* **2008**, *89*, 567–573. [[CrossRef](#)]
6. Ahmed, M.S.; Attia, Y.A. Aerogel materials for photocatalytic detoxification of cyanide wastes in water. *J. Non-Cryst. Solids* **1995**, *186*, 402–407. [[CrossRef](#)]
7. Saputera, W.H.; Rizkiana, J.; Wulandari, W.; Sasongko, D. Role of defects on TiO₂/SiO₂ composites for boosting photocatalytic water splitting. *RSC Adv.* **2020**, *10*, 27713–27719. [[CrossRef](#)]
8. Guan, K. Relationship between photocatalytic activity, hydrophilicity and self-cleaning effect of TiO₂/SiO₂ films. *Surf. Coat. Technol.* **2005**, *191*, 155–160. [[CrossRef](#)]
9. Yuranova, T.; Mosteo, R.; Bandara, J.; Laub, D.; Kiwi, J. Self-cleaning cotton textiles surfaces modified by photoactive SiO₂/TiO₂ coating. *J. Mol. Catal. A Chem.* **2006**, *244*, 160–167. [[CrossRef](#)]
10. Jacobs, G.; Das, T.K.; Zhang, Y.; Li, J.; Racoillet, G.; Davis, B.H. Fischer–Tropsch synthesis: Support, loading, and promoter effects on the reducibility of cobalt catalysts. *Appl. Catal. A Gen.* **2002**, *233*, 263–281. [[CrossRef](#)]
11. Pizzio, L.; Cáceres, C.; Blanco, M. Acid catalysts prepared by impregnation of tungstophosphoric acid solutions on different supports. *Appl. Catal. A Gen.* **1998**, *167*, 283–294. [[CrossRef](#)]
12. Limo, M.J.; Rabada, A.S.; Boix, E.; Thota, V.; Westcott, Z.C.; Puddu, V.; Perry, C.C. Interactions between Metal Oxides and Biomolecules: From Fundamental Understanding to Applications. *Chem. Rev.* **2018**, *118*, 11118–11193. [[CrossRef](#)]
13. Chen, R.-F.; Zhang, C.-X.; Deng, J.; Song, G.-Q. Preparation and photocatalytic activity of Cu²⁺-doped TiO₂/SiO₂. *Int. J. Miner. Met. Mater.* **2009**, *16*, 220–225. [[CrossRef](#)]
14. Shishmakov, A.B.; Kharchuk, V.G.; Kuznetsova, O.V.; Mikushina, Y.V.; Koryakova, O.V.; Kovaleva, E.G.; Petrov, L.A.; Molochnikov, L.S.; Chupakhin, O.N. The activity of element dioxides in liquid-phase oxidation of 2,3,5-trimethyl-1,4-hydroquinone. *Russ. J. Phys. Chem. A* **2003**, *77*, 623–628.
15. Parshina, E.V.; Molochnikov, L.S.; Kovaleva, E.; Shishmakov, A.B.; Mikushina, Y.V.; Kirilyuk, I.; Grigor'Ev, I.A. Medium acidity and catalytic properties of composite materials based on silica and titania and powder cellulose in the presence of Cu²⁺ ions. *Russ. J. Phys. Chem. A* **2011**, *85*, 452–456. [[CrossRef](#)]
16. Shishmakov, A.B.; Molochnikov, M.S.; Antonov, D.O.; Koryakova, O.V.; Seleznev, A.S.; Petrov, L.A. Synthesis of Cu(II)-containing TiO₂-SiO₂ binary xerogels by hydrolysis of a mixture of tetrabutoxytitanium, tetraethoxysilane, and copper(II) chloride in a water-ammonia atmosphere. *Russ. J. Appl. Chem.* **2013**, *86*, 297–303. [[CrossRef](#)]
17. Shishmakov, A.B.; Molochnikov, L.S.; Antonov, D.O.; Koryakova, O.V.; Mikushina, Y.V.; Petrov, L.A. Synthesis of TiO₂-SiO₂ and TiO₂-SiO₂-Cu(II) xerogels by cohydrolysis of precursors in the absence of a solvent and redox catalysts. *Russ. J. Inorg. Chem.* **2014**, *59*, 159–165. [[CrossRef](#)]
18. Teichner, S.; Nicolaon, G.; Vicarini, M.; Gardes, G. Inorganic oxide aerogels. *Adv. Colloid Interface Sci.* **1976**, *5*, 245–273. [[CrossRef](#)]
19. Itoh, M.; Hattori, H.; Tanabe, K. The acidic properties of TiO₂-SiO₂ and its catalytic activities for the amination of phenol, the hydration of ethylene and the isomerization of butene. *J. Catal.* **1974**, *35*, 225–231. [[CrossRef](#)]
20. Snyder, L.R.; Ward, J.W. The Surface Structure of Porous Silicas. *J. Phys. Chem.* **1966**, *70*, 3941–3952. [[CrossRef](#)]
21. Auroux, A.; Brait, A.; Brunner, E.; Fajula, F.; Garrone, E.; Jentys, A.; Lercher, J.; Pfeifer, H. *Acidity and Basicity*; Springer: Berlin/Heidelberg, Germany, 2008. [[CrossRef](#)]
22. Kladnig, W.F. Use of Hammett indicators for acidity measurements in zeolites. *J. Phys. Chem.* **1979**, *83*, 765–766. [[CrossRef](#)]
23. Védrine, J.C. Acid–base characterization of heterogeneous catalysts: An up-to-date overview. *Res. Chem. Intermed.* **2015**, *41*, 9387–9423. [[CrossRef](#)]
24. Khramtsov, V.; Marsh, D.; Weiner, L.; Reznikov, V. The application of pH-sensitive spin labels to studies of surface potential and polarity of phospholipid membranes and proteins. *Biochim. Biophys. Acta (BBA) Biomembr.* **1992**, *1104*, 317–324. [[CrossRef](#)]
25. Smirnova, T.I.; Voinov, M.A.; Smirnov, A. Spin Probes and Spin Labels. In *Encyclopedia of Analytical Chemistry: Applications, Theory and Instrumentation*; John Wiley & Sons, Ltd.: Chichester, UK, 2009; p. 31. [[CrossRef](#)]
26. Kovaleva, E.G.; Molochnikov, L.S.; Venkatesan, U.; Marek, A.; Stepanova, D.P.; Kozhikhova, K.V.; Mironov, M.A.; Smirnov, A.I. Acid–Base Properties of Nanoconfined Volumes of Anodic Aluminum Oxide Pores by EPR of pH-Sensitive Spin Probes. *J. Phys. Chem. C* **2016**, *120*, 2703–2711. [[CrossRef](#)]
27. Kirilyuk, I.A.; Bobko, A.A.; Khramtsov, V.V.; Grigor'Ev, I.A. Nitroxides with two pK values—useful spin probes for pH monitoring within a broad range. *Org. Biomol. Chem.* **2005**, *3*, 1269–1274. [[CrossRef](#)]
28. Bobko, A.; Dhimitruka, I.; Komarov, D.A.; Khramtsov, V.V. Dual-Function pH and Oxygen Phosphonated Trityl Probe. *Anal. Chem.* **2012**, *84*, 6054–6060. [[CrossRef](#)] [[PubMed](#)]
29. Shishmakov, A.B.; Mikushina, Y.V.; Koryakova, O.V.; Valova, M.S.; Petrov, L.A.; Melkozerov, S.A. Synthesis of TiO₂-SiO₂ xerogels via the hydrolysis of a tetrabutoxytitanium-tetraethoxysilane mixture in aqueous ammonia and hydrochloric acid atmospheres. *Russ. J. Inorg. Chem.* **2012**, *57*, 787–793. [[CrossRef](#)]
30. Molochnikov, L.S.; Kovaleva, E.; Golovkina, E.L.; Kirilyuk, I.; Grigor'Ev, I.A. Spin probe study of acidity of inorganic materials. *Colloid J.* **2007**, *69*, 769–776. [[CrossRef](#)]
31. Kovaleva, E.G.; Molochnikov, L.S.; Golovkina, E.L.; Hartmann, M.; Kirilyuk, I.A.; Grigor'Ev, I.A. Dynamics of pH-sensitive nitroxide radicals in water adsorbed in ordered mesoporous molecular sieves by EPR Spectroscopy. *Microporous Mesoporous Mater.* **2013**, *179*, 258–264. [[CrossRef](#)]

32. Molochnikov, L.S.; Kovalyova, E.G.; Grigor'Ev, I.A.; Reznikov, V.A. Determination of Acidity in the Interior of the Cross-Linked Polyelectrolyte Grain by the Use of pH-Sensitive Probes. In *Metal-Containing Polymeric Materials*; Springer: Boston, MA, USA, 1996; pp. 395–401. [[CrossRef](#)]
33. Kovaleva, E.G.; Molochnikov, L.S.; Golovkina, E.L.; Hartmann, M.; Kirilyuk, I.A.; Grigoriev, I.A. Electrical potential near hydrated surface of ordered mesoporous molecular sieves assessed by EPR of molecular pH-probes. *Microporous Mesoporous Mater.* **2015**, *203*, 1–7. [[CrossRef](#)]
34. Parks, G.A. *Aqueous Surface Chemistry of Oxides and Complex Oxide Minerals: Isoelectric Point and Zero Point of Charge*; American Chemical Society: Washington, DC, USA, 1967; pp. 121–160. [[CrossRef](#)]
35. Crocker, M.; Herold, R.H.M.; Wilson, A.E.; Mackay, M.; Emeis, C.A.; Hoogendoorn, A.M. ¹H NMR spectroscopy of titania. Chemical shift assignments for hydroxy groups in crystalline and amorphous forms of TiO₂. *J. Chem. Soc. Faraday Trans.* **1996**, *92*, 2791–2798. [[CrossRef](#)]
36. Antonov, D.; Kovaleva, E.; Molochnikov, L.; Shishmakov, A. Surface electrical potential of ZrO₂-SiO₂ binary xerogels by EPR pH-sensitive spin probes. In *AIP Conference Proceedings*; AIP Publishing LLC: Yekaterinburg, Russia, 2019; Volume 2063, p. 040001. [[CrossRef](#)]
37. Molochnikov, L.S.; Kovalyova, E.G.; Grigor'Ev, I.A.; Zagorodni, A.A. Direct Measurement of H⁺ Activity inside Cross-Linked Functional Polymers Using Nitroxide Spin Probes. *J. Phys. Chem. B* **2003**, *108*, 1302–1313. [[CrossRef](#)]
38. Kovaleva, E.G.; Molochnikov, L.S.; Stepanova, D.P.; Pestov, A.V.; Trofimov, D.G.; Kirilyuk, I.A.; Smirnov, A.I. Interfacial Electrostatic Properties of Hydrated Mesoporous and Nanostructured Alumina Powders by Spin Labeling EPR. *Cell Biophys.* **2016**, *75*, 159–170. [[CrossRef](#)]
39. Budil, D.; Lee, S.; Saxena, S.; Freed, J.H. Nonlinear-Least-Squares Analysis of Slow-Motion EPR Spectra in One and Two Dimensions Using a Modified Levenberg–Marquardt Algorithm. *J. Magn. Reson. Ser. A* **1996**, *120*, 155–189. [[CrossRef](#)]